Journal of Non-Crystalline Solids 356 (2010) 1679–1688

Contents lists available at ScienceDirect

Journal of Non-Crystalline Solids

journal homepage: www.elsevier.com/ locate/ jnoncrysol

Stress induced pore formation and phase selection in a crystallizing stretched glass

Vladimir M. Fokin [a,b,*], Alexander S. Abyzov [c], Jürn W.P. Schmelzer [d], Edgar D. Zanotto [b]

[a] Vavilov State Optical Institute, ul. Babushkina 36-1, 193 171 St. Petersburg, Russia
[b] Vitreous Materials Laboratory, Department of Materials Engineering, Federal University of São Carlos, UFSCar, 13565-905, São Carlos-SP, Brazil
[c] National Science Center, Kharkov Institute of Physics and Technology, Academician Street 1, 61108 Kharkov, Ukraine
[d] Institut für Physik, Universität Rostock, 18051 Rostock, Germany

ARTICLE INFO

Article history:
Received 9 December 2009
Received in revised form 28 May 2010
Available online 17 July 2010

Keywords:
Glass;
Crystallization;
Stress;
Nucleation;
Pore

ABSTRACT

In this article we experimentally investigate and theoretically describe phase selection and the nucleation of pores in small samples of undercooled diopside liquid when it is enclosed by a hard crystalline surface layer. The formation of the surface crystalline layer begins with nucleation and growth of highly dense diopside crystals. At the moment of impingement of these crystals on the sample surface, the crystallization pathway switches from diopside to a wollastonite-like (WL) phase. The WL crystal produces less elastic stress energy than diopside due to its lower density, which is closer to the liquid density. The relative content of the two crystalline phases can be changed by varying the sample size. Due to the density misfit, the growth of the WL crystalline layer leads to uniform stretching of the encapsulated liquid and finally to formation of one pore, which rapidly grows up to a size that almost eliminates the elastic stress and, therefore, dramatically reduces the driving force for pore nucleation. This nucleation process occurs in a very narrow range of negative pressures indicating that it proceeds via homogeneous nucleation. This result is corroborated by theoretical calculations of elastic stress fields and their effect on nucleation. Good qualitative and partial quantitative agreement between experiment and theory is found. The findings of this research are quite general because the densities of most glasses significantly differ from those of their isochemical crystals, and are thus of technological significance for glass–ceramic development and sinter-crystallization processes.

1. Introduction

External pressure [1] or internally induced elastic stresses [2] – which arise during crystallization of glass-forming liquids due to the difference between the densities of the original glass and newly formed crystals – may strongly affect the kinetics of phase transitions in condensed systems and, as will be shown here, may trigger the precipitation of new phases that do not commonly develop at the respective values of pressure and temperature. In addition, these stresses can also induce vacuum pore (void) nucleation.

In previous works, the influence of internal elastic stresses on crystal nucleation and growth rates in glasses was considered from both theoretical and experimental points of view [3–7]. Here we focus onto two different aspects of elastic stress effects; we will show that, besides their effect on crystallization kinetics, elastic stresses may affect the crystallization pathways and may result, similarly to segregation processes of dissolved gases in liquids or solids, and especially cavitation processes in liquids, in the formation of *pores* in crystallizing glass samples. These pores are formed to compensate, at least partly, the elastic strains caused by the density difference between glass and crystal phase. The formation of pores is typical in glass crystallization if isolated areas of a residual glass phase crystallize, e.g., in the case of surface crystallization during sintering of glass powders. Hence, in addition to its scientific importance, the problem of pore formation in glass–ceramics is a theme of considerable technological significance.

In the following analysis we consider the situation that a crystalline layer is formed on the surface of a glass particle, i.e., we consider particles of a glass powder or other particles with isometric form, such as spheres or cubes. The formation of such crystalline surface layer can fix, like a nutshell, the total volume of the system that then leads (in further crystallization) to uniform stretching of both crystal and residual glass that is enclosed by the crystalline layer. The crystalline layer does not allow the stresses to relax and thus elastic stress energy accumulates in such stretched system. The elastic energy reduces the thermodynamic driving force for crystallization. In this way, the evolution of elastic stresses inhibits and even may fully terminate crystal growth.

There exists, however, another possible way of evolution in which the system may react to elastic stress fields; i.e. by the formation of pores inside the liquid regions encapsulated by the crystalline layer. In the course of development of a crystalline layer on the sample surface, the remnant liquid is uniformly stretched. As a result, similar to cavitation processes in liquids, pores may spontaneously evolve.

* Corresponding author. Vavilov State Optical Institute, ul. Babushkina 36-1, 193 171 St. Petersburg, Russia.
E-mail address: vfokin@pisem.net (V.M. Fokin).

0022-3093/$ – see front matter © 2010 Elsevier B.V. All rights reserved.
doi:10.1016/j.jnoncrysol.2010.06.008

Hence, in this case, the elastic stress energy in the glass is the origin of pore nucleation. Thus we will be dealing with nucleation of pores in a stretched liquid. According to the principle of le Chatelier–Brown this process reduces the intensity of elastic stresses (which arise due to the density difference between the crystalline and liquid parts of system).

In the described crystallization pathway, further growth of the crystalline layer is accompanied by an increase of the pore volume. By this reason, elastic stresses will then decay. Thus a distinctive feature of this nucleation process is that, in the general case, a second pore does not form since the first one almost eliminates the stretching of the residual liquid and the thermodynamic driving force for pore formation. Thus, a theoretical treatment of pore nucleation can be performed in terms of determining the waiting time for the appearance of the first pore as, e.g., in the case of crystallization of metal droplets [8] or boiling of liquids [9] following, with some modifications, the basic ideas of the classical nucleation theory [8–11].

It should be noted that classical nucleation theory has been successfully applied to the description of pore formation in elastic solids under load, which leads to cracks and destruction of the material [12,13], i.e. to effects which from their physical origin are somewhat similar to the processes discussed here. However, to the best of our knowledge, the nucleation approach has not been applied yet to pore formation caused by crystallization of glass-forming melts. The aim of the present paper is thus to fill this gap and to apply the modified theory to the analysis of experimental data on pore nucleation. All mentioned aspects make the effects of elastic stresses of great important for the development and manufacture of glass–ceramics (cf. also [14]), especially for sinter-crystallization processes.

This paper is organized as follows: in Section 2 results of experimental studies of vacuum pore formation in a glass sample strained by surface crystallization are outlined. In addition, we present data on the sequence of appearance of different crystalline phases formed. As will be shown, the formation of different phases can be understood as a special case of phase selection triggered by elastic stresses. To interpret quantitatively the respective data (Section 2), we employ the recently developed theory of elastic stresses in finite spherical domains [15,16]. Theoretical results are incorporated here into the description of pore nucleation kinetics in the system under investigation (Section 3). A summary and an analysis of further possible developments complete the paper.

2. Experiments

2.1. Material and methods

Diopside ($CaO \cdot MgO \cdot 2SiO_2$) glass was chosen as a model for the analysis due to the very high difference between the densities of diopside crystal, ρ_{cr}, and diopside glass, ρ_{gl}. This density difference corresponds to a value of the density misfit parameter, δ, equal to

$$\delta = \frac{\rho_{cr} - \rho_{gl}}{\rho_{gl}} \sim 0.16.$$

This parameter determines the magnitude of the elastic stresses in the crystallization process studied.

The glass was melted in a platinum crucible at about 1500 °C in an electric furnace in air. Analytic grade carbonates of calcium and magnesium and anhydrous amorphous silicon dioxide were used for the synthesis. The melt was cast into a massive steel plate. To eliminate a few bubbles detected by optical microscopy in the polished glass plates, the melting procedure was repeated at 1550 °C for 5 h. After re-melting and annealing at T close to the glass transition temperature T_g, no bubbles were observed within the resolution limit of an optical microscope (~1 μm). This glass was used to study pore formation.

Opposite to the glass obtained via single melting, after proper heat-treatment above T_g the re-melted glass revealed a few spherulites in its interior, with a number density not higher than 0.2 mm^{-3}. However, it is well-known that diopside glass crystallizes only from the surface, as indeed observed for the single-melted glass. This means that during re-melting some impurities dropped into the melt acting as active centers for crystal nucleation. Nevertheless, neither the growth rate of the crystalline surface layer nor the glass transition temperature differs from that of single-melted glass. Thus, we neglected the above mentioned impurities.

Luckily, however, these (unknown) impurities gave us the unique possibility to measure the growth rate of the crystalline phase in the glass interior. Since we employed glass samples with a volume not smaller than 8 mm^3, the total volume of the crystals inside the sample can be neglected if compared to that of the crystalline surface layer. It should also be noted that the absence of detectable volume nucleation in pure diopside glass is possibly determined by the strong elastic stresses (which decrease the thermodynamic driving force for crystallization and suppress homogeneous nucleation in the glass volume, cf. e.g. [3,4]).

The compositions of the studied glass, before and after re-melting, are shown in Table 1. Within the accuracy of the analysis [about 0.3–0.4 mol%] they are close to each other and to that of stoichiometric diopside. The composition of the re-melted glass is noted in the phase diagram (see Fig. 1).The glass samples were cut by a diamond saw as cubes with sides a equal to about 2, 3, and 4 mm, respectively. Such cubes were then dropped into a previously stabilized vertical box furnace. Opposite to the crystallization behavior of any polished surface, crystalline surface layers on the cube surfaces quickly formed due to the presence of many active centers for nucleation. After a given period of time, the samples were quenched to room temperature. Then the top and bottom surfaces of the cubes were eliminated by grinding and polishing to study their interior and to measure the crystalline layer thickness using an optical microscope (Leica DMRX coupled with a Leica DFC490 CCD camera).

Optical microscopy and X-ray analysis were employed to identify the crystalline phases. X-ray diffraction measurements were carried out on the powdered samples using a Siemens D5005 X-ray diffractometer operating at 40 mA and 40 kV. CuK_α (1.5406 Å) was employed as incident radiation. A Netzsch 404 Differential Scanning Calorimeter (DSC) was used to detect glass–crystal and crystal–crystal transitions.

2.2. Results

2.2.1. Crystalline phases

As already mentioned, the dominating type of crystallization of the studied glass is surface crystallization. Two crystal morphologies were observed by optical microscopy on the cross sections of the large bulk (regular shaped) and the small (powdered) samples. The first type of crystals is square faceted (Fig. 2a, b, *1*) whereas the second formed a relatively dense layer (Fig. 2a, b, *2*) with the crystal/glass interface parallel to the external boundaries of the sample. The latter feature is clearly seen in samples with planar surfaces (Fig. 2a).

The growth of the first type of crystals was terminated by the formation of the second. The sequence of occurrence of the different crystalline phases is illustrated in Fig. 3. This fact allowed us to vary the ratio between these kinds of crystals by changing the shape and

Table 1
Nominal and analysed glass compositions.

	SiO_2	CaO	MgO
	mol%		
Original glass	50.9	24.4	24.7
Glass after re-melting	50.5	25.8	23.7
$CaO \cdot MgO \cdot 2SiO_2$	50.0	25.0	25.0

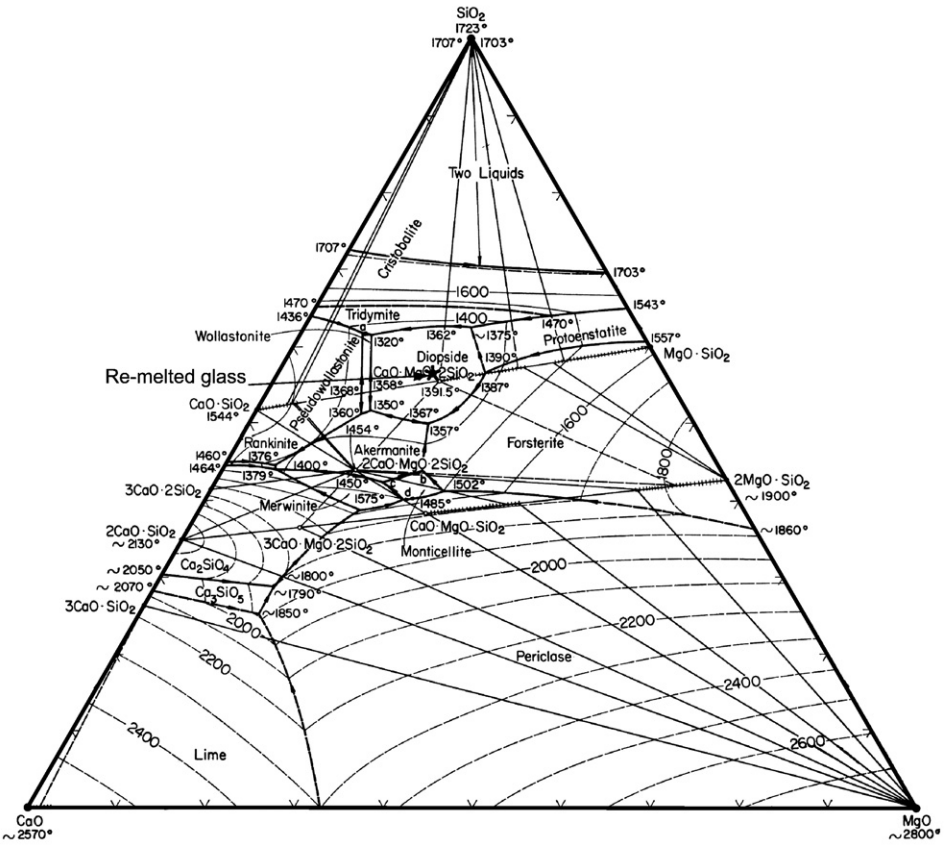

Fig. 1. Phase diagram of CaO–MgO–SiO_2 system [17]. Star denotes composition of re-melted glass. Compositions are given in wt.%.

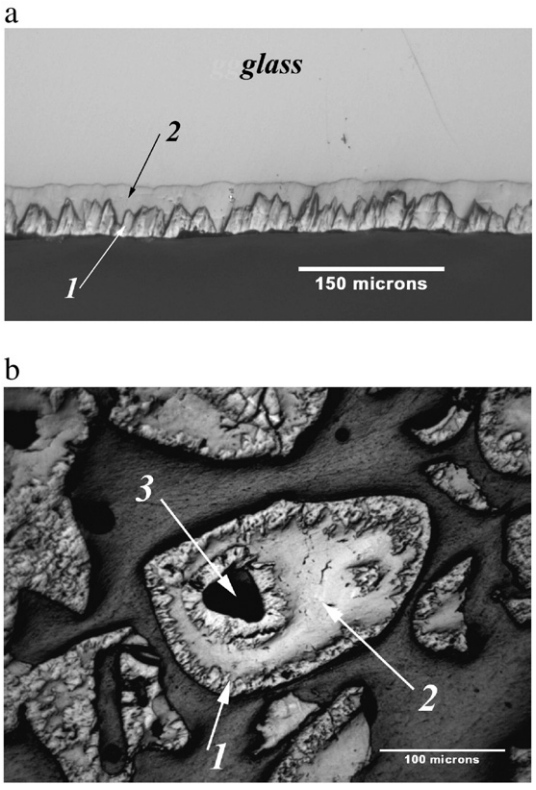

Fig. 2. Reflected light optical micrographs of crystallizing bulk (a) and powder (b) diopside glass samples heat-treated at 870 °C for 90 min and at 850 °C for 50 min, respectively. Arrows *1* and *2* refer to diopside and wollastonite-like crystals, arrow *3* shows the location of a pore.

size of the glass samples before crystallization. It is reasonable to expect that crystallization of a bulk glass sample produces more of the second type of crystals than crystallization of a glass powder.

Fig. 4 shows X-ray diffraction spectra of a glass powder with an average size of about 60 μm and (3×1.5×7 mm) bulk glass crystallized at 850 °C for 24 and 120 h, respectively. This bulk sample revealed only surface crystallization. It should be noted that 120 h of heat-treatment at 850 °C was not sufficient for full crystallization of the monolithic sample (please see the weak halo of the amorphous phase in Fig. 4b). The spectrum of the crystallized glass powder matches that of diopside [75–1072], while the spectrum of the crystallized bulk glass is similar to that of wollastonite [72–2284] with the distinction that the peaks shift to higher angles. Thus, we can suppose that the second phase is a solid solution with the wollastonite structure, where half Ca is substituted by Mg. This phase can be treated as a phase having a structure similar to that of the low or high temperature forms of wollastonite, with the following cell parameters: low temperature triclinic a/b/c/7.605/7.049/6.822 Å; α/β/γ 90.39/95.08/103.16(°); $Z=3$ and high temperature monoclinic a/b/c/14.80/7.048/6.8221 Å; α/β/γ 90/95.08/90(°); $Z=6$. The X-ray densities of these supposed structures were calculated as

$$\rho = 1.6602ZM / V, \tag{1}$$

where M is the molar weight of diopside and V is the volume of a cell given by

$$V = abc\left[\sqrt{1-\cos(\alpha)^2-\cos(\beta)^2-\cos(\gamma)^2+2\cos(\alpha)\cos(\beta)\cos(\gamma)}\right]. \tag{2}$$

The respective values of ρ are: $\rho_{tric}=3.042$ g/cm^3 and $\rho_{mono}=3.058$ g/cm^3, respectively.

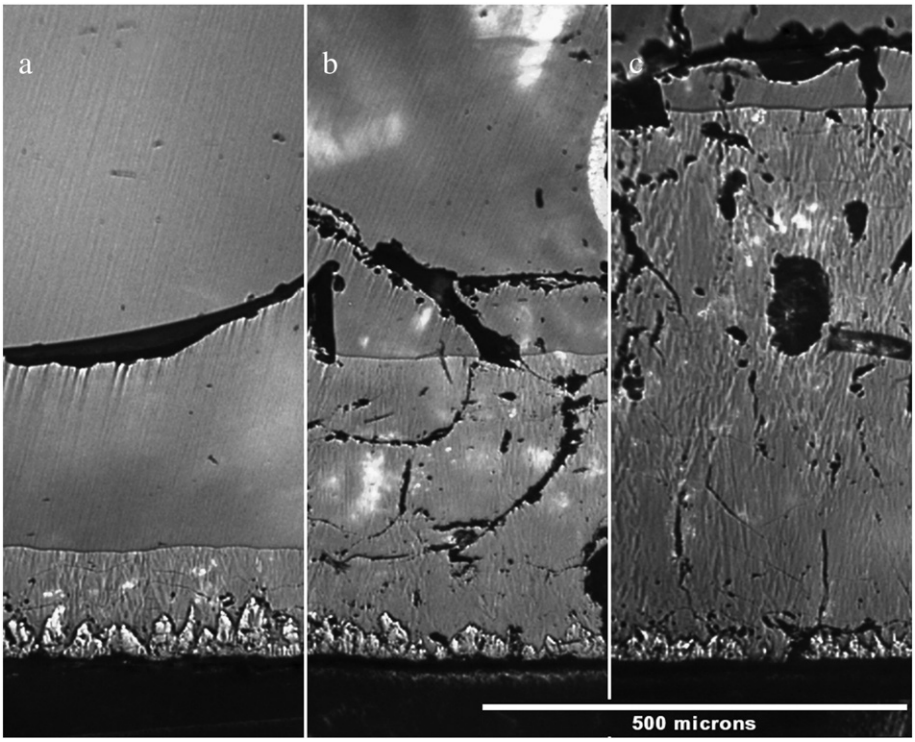

Fig. 3. Reflected light optical micrographs of cross sections of bulk diopside glass samples heat-treated at 870 °C for 7 (a), 14 (b), and 24 (c) hours.

As we mentioned before, some samples of the re-melted glass revealed a few spherulites in the interior after proper heat-treatment. According to an X-ray analysis these spherulites are also a wollastonite-like phase as the second phase in the crystalline surface layer. The X-ray diffraction spectrum of the internal part of the diopside glass sample (see inset of Fig. 5), crystallized at 870 °C for 8 h and including a few spherulites, is shown in Fig. 5 together with the diffraction spectrum of the wollastonite-like phase taken from Fig. 4b.

The sequence of crystal phase formation and the effect of sample shape on phase composition were corroborated by DSC analysis. Fig. 6 shows the heating and cooling DSC runs of bulk and powder glasses (Fig. 6a) and samples preliminary crystallized using bulk and powder glass (Fig. 6b). The DSC curve of the powdered glass has only one exothermic peak, which according to X-ray data refers to diopside crystallization. We recall that diopside crystals are the first phase forming on the glass surface, and in the case of small powder particles it is the main or unique crystalline phase. Opposite to powdered glass, the DSC curve of the bulk glass reveals two exothermic peaks. As was shown in Figs. 3, 4 the main crystalline phase in the crystallized bulk sample is represented by the second type of crystals (wollastonite-like phase). Hence we could interpret the first peak as crystallization of the wollastonite-like phase and the second peak close to 1100 °C as its transformation into diopside. Since diopside is the stable phase in a non-stretched system, the cooling curves of both powder and bulk samples do not reveal any thermal effects.

The above discussed effect of sample shape and size on the type of the crystal phases which occur is also confirmed by DSC measurements of preliminary crystallized powder glass and bulk glass (Fig. 6b). The curve of the crystallized powder glass does not reveal any thermal effects since the latter consists of diopside crystals, while the curve of a monolithic piece previously crystallized at a relatively low temperature shows an exothermic peak at about 1100 °C that is caused by the transition of a wollastonite-like phase into diopside. But a DSC-scan of a sample preliminary crystallized at 1200 °C does not reveal any peaks independent of its shape.

Fig. 7 shows the thickness of the crystalline surface layer, h, *versus* time at $T = 870$ °C; vacuum pore (void) formation was studied at this temperature. As we already mentioned, with a proper heat-treatment, re-melted diopside glass reveals sometimes a few internal wollastonite-like crystals with spherulitic form, which have no effect on the results of the present analysis and, by this way, were not studied in detail. However, we used the sample of re-melted glass which revealed some spherulites in the interior to measure the size evolution of a given spherulite with heat-treatment time. Fig. 8 presents the radii of nine spherulites together with h as a function of time of heat-treatment at 870 °C. One can see that the rate of crystal growth of the crystalline layer is practically equal to that of the spherulites. This result is explained by the X-ray analysis data; both are wollastonite-like crystals. It should be noted also that spherulite growth generally starts somewhat later than that of the crystalline layer, see a double ended arrow in Fig. 8.

2.2.2. Pores

Cubic samples with sides of size a of about 2, 3, and 4 mm were cut from the re-melted diopside glass and heat-treated at 870 °C for different times. Then the crystalline layers were removed from two parallel sides by grinding and polishing to measure the layer thickness, h, and to check whether pores had been formed in their volume. A dimensionless parameter X was used to characterize the condition of pore nucleation. This parameter is defined as

$$X = \frac{a-2h}{a}. \tag{3}$$

The values of X vary from 1 (absence of a crystalline layer) to 0 (fully crystallized sample). The latter case was never realized in our experiments due to the formation of pores. As was shown in refs. [15,16] the value of the parameter X determines the degree of elastic stresses in a finite system of the considered geometry.

The growth of the crystalline layer results in stretching the residual liquid inside the cube and finally in the formation of pores via nucleation and fast growth up to a volume that compensates the density difference between the amorphous and crystalline phases. Thus it is reasonable to suppose that pore nucleation is the limiting

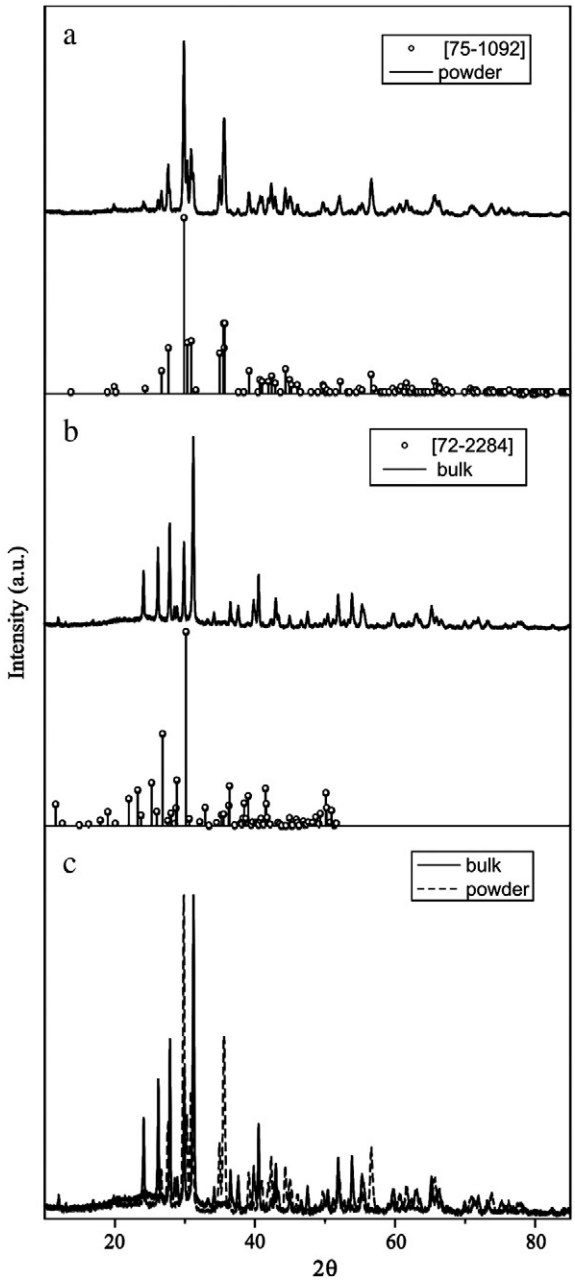

Fig. 4. X-ray diffraction spectra of diopside powder (a) and bulk (b) glass crystallized at 850 °C for 24 h and 120 h, respectively. Both spectra are presented in the Fig. 4c.

process. The peculiarity of this nucleation process is that, as a rule, a second pore does not appear since fast growth of the first eliminates the elastic stresses. Thus, the nucleation experiment is reduced to the detection of the first pore.

Fig. 9 shows the statistical results of pore detection as a function of the parameter *X*. These data refer to cubes of different sizes. According to Fig. 9, nucleation of a pore occurs in a very narrow interval of *X*-values. The average value of *X* at which a pore nucleates is marked by X_*. We interpret the existence of such narrow interval of *X*-values for the occurrence of pores as a strong indication that pores homogeneously nucleate [18].

In such an interpretation, we connect the possibility of pore observation with its nucleation and growth. Alternatively, one could suppose that at high values of *X*, i.e. at $X_* < X < 1$, the pore has a size that is too small for detection by optical microscopy. To eliminate this doubt we calculated the diameter of a pore, *D*, which has to

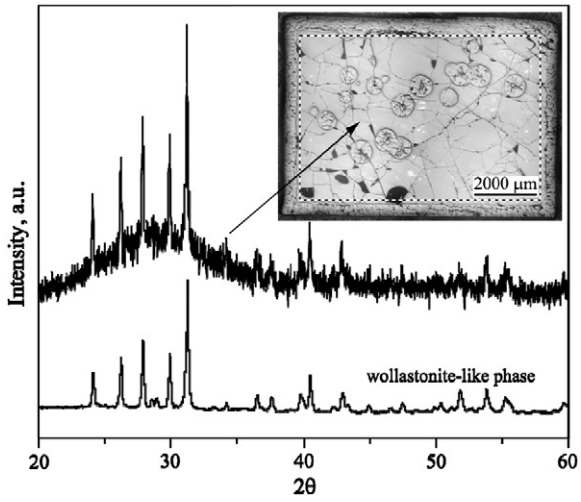

Fig. 5. X-ray diffraction spectra of the internal part (see inset of sample cross section) of monolithic samples (4×7×9 mm) of re-melted diopside glass crystallized at 870 °C for 8 h (upper spectrum) and wollastonite-like phase (lower spectrum).

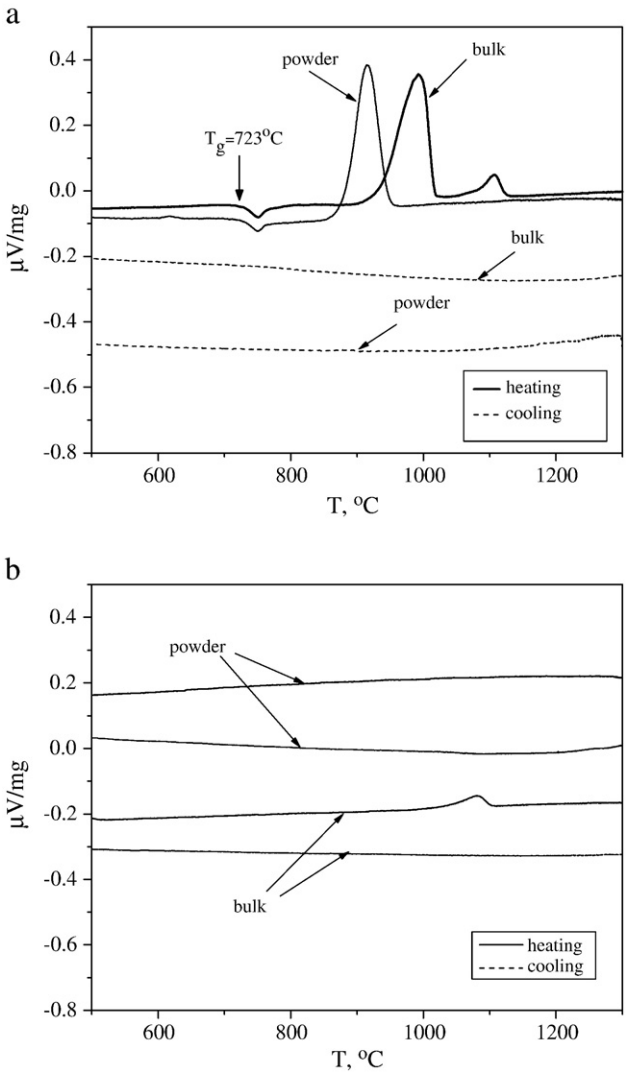

Fig. 6. DSC heating and cooling curves: the experiments were performed at $C = 10$ K/min for (a) bulk (~4 mm) and powder (~200 μm) glass and (b) crystallized powder (<60 μm) and bulk (~7×5×2 mm) glass at 850 °C for 24 h and 219 h, respectively.

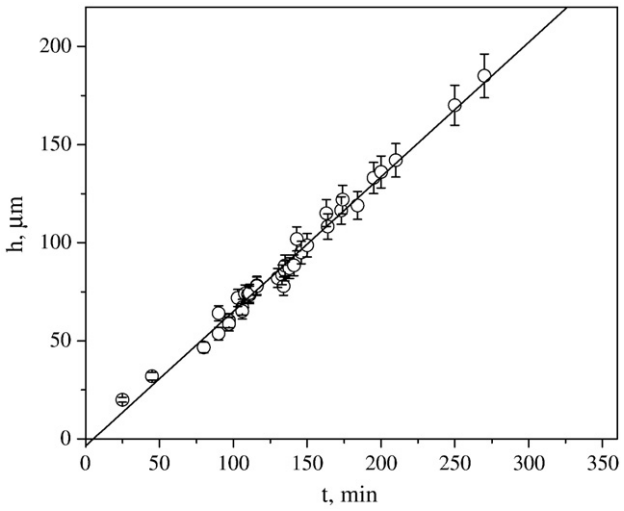

Fig. 7. Thickness of the crystalline layer as a function of heat-treatment time at 870 °C.

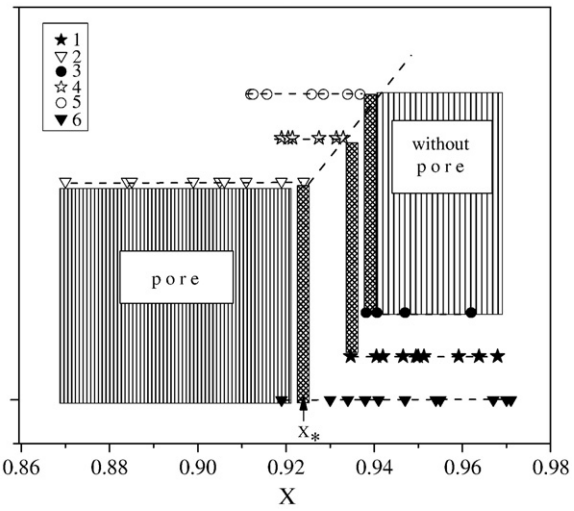

Fig. 9. Schematic representation of pore nucleation data. Black and white symbols refer to samples without and with a pore, respectively. The experiments were performed at $T = 870$ °C for samples with the following values of the size parameter a: (1, 2) $a = 1.94$ mm; (3, 4) $a = 2.99$ mm; (5, 6) $a = 3.91$ mm.

compensate the density mismatch for different X. The respective value can be easily obtained taking into account that the volume of the pore is equal to the volume of the crystalline phase multiplied be the misfit parameter, δ. We then get the following dependence for the pore diameter D as a function of X:

$$D = a\left\{\frac{6}{\pi}\delta\left[1-X^3\right]\right\}^{1/3}. \quad (4)$$

According to Fig. 10, the expected diameter of a pore at values of X of the order of 0.93–0.97 should be larger than the resolution limit of optical microscopy. This result indeed means that pores do not form until X achieves some critical value, X_*. Fig. 11 shows that the value of X_* grows with an increase of the cube volume. Sometimes, some (hypothetically diopside) crystals are formed on the pore surface (Fig. 12).

3. Theoretical interpretation and discussion

The following main experimental results will be discussed: i) the switch from one to another crystalline phase during phase transition and the possibility to affect the type of phase developing by changing the size of the glass samples, and ii) the formation of pores at an relatively early stage of crystallization within a narrow interval of X. Both groups of results will be interpreted in terms of the influence of elastic stresses.

3.1. Sequence of appearance of crystalline phases

As discussed in the outline of the experimental results, diopside first forms and is then replaced by a wollastonite-like phase. In order to give an interpretation of the origin of this sequence of formation of different crystalline phases, the following fact is very important: the density of the wollastonite-like phase is considerably lower than that of diopside crystals. Thus, the density misfit and the resulting elastic stress effect in the crystallization process for the wollastonite-like phase are lower than that for diopside.

Table 2 shows the respective values of ρ, δ, and δ^2. Since the total energy of elastic deformation is proportional to δ^2, the effects of elastic stresses on nucleation and growth of the wollastonite-like crystals must be less than those for diopside by a factor of about 5. This elastic

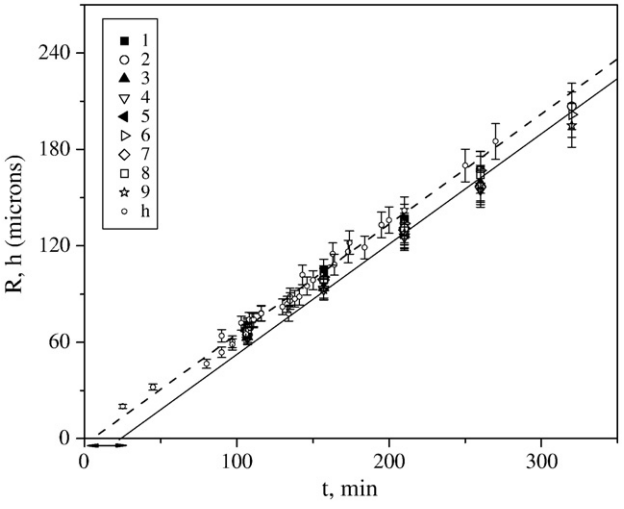

Fig. 8. The radii of spherulites (1–9) *versus* time of heat-treatment at 870 °C. The solid line is a linear fit of the respective data, while the dotted line is a linear fit of the $h(t)$-data shown also in Fig. 7.

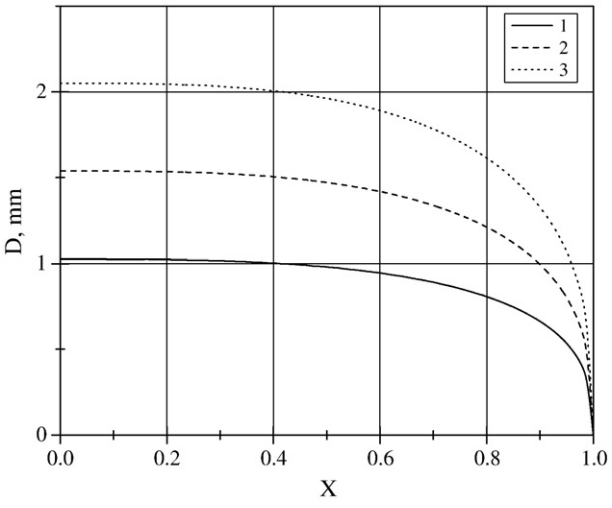

Fig. 10. Diameter of a pore calculated by Eq. (4) and using the density of the wollastonite-like phase (see Table 2) in dependence on the parameter X for cubes with sides 2 mm (*1*), 3 mm (*2*), and 4 mm (*3*).

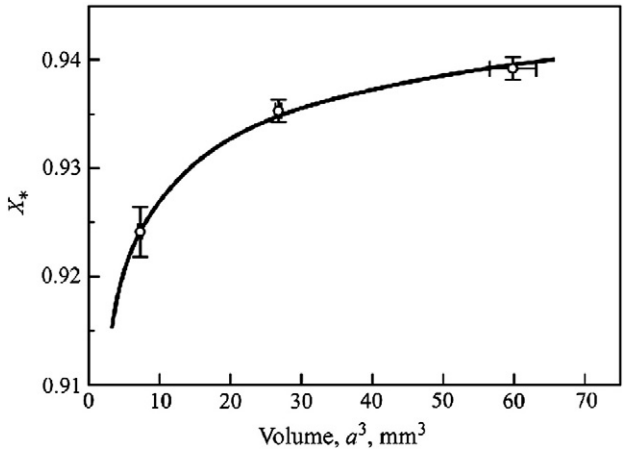

Fig. 11. Critical value of X *versus* volume of the sample. Circles show experimental data for $T=870$ °C. Curve is calculated for sphere with $R_3=a/2$.

strain energy must be taken into account to estimate the effective thermodynamic driving force for crystallization as

$$\Delta G^{eff} = \Delta G - \Delta f, \tag{5}$$

where ΔG is the thermodynamic driving force for crystallization of the non-stressed glass and Δf is the difference between the densities f_{cr} and f_m of elastic deformation energy, F, in a stretched crystal and melt, respectively, i.e.

$$\Delta f = f_{cr} - f_m. \tag{6}$$

The value of Δf increases with the growth of the crystalline layer and hence with a decrease of the parameter X faster in the case of diopside than in the case of the wollastonite-like phase. Thus the effective thermodynamic driving force for crystallization of diopside has to decrease with decreasing X faster than that for the wollastonite-like phase. This difference determines the switching at $X=X_{d/w}$ of the type of crystalline phases growing in the system.

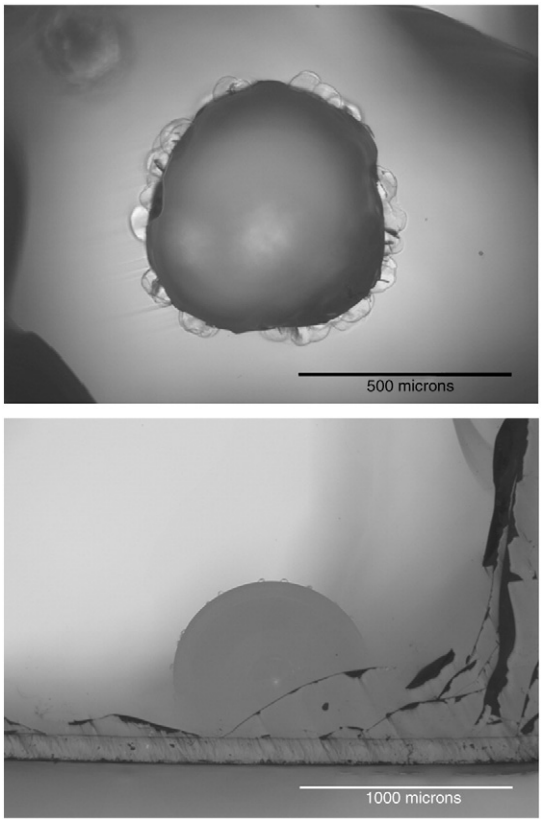

Fig. 12. Transmitted light optical micrographs of diopside glass heat-treated at 870 °C for 200 min (top) and at 890 °C for 64 min (bottom).

Table 2
Densities and density misfits for different crystalline phases.

Phase	Density g/cm^3	δ	δ^2
Diopside crystal	3.29 [19]	0.1584	0.025
Wollastonite-like crystal, triclinic	3.04	0.0704	0.005
Wollastonite-like crystal, monoclinic	3.06	0.0775	0.006
Diopside glass	2.84 [20]		

To illustrate this effect, the evolution of Δf was calculated employing the analytical results obtained in refs. [15,16] for the case of surface crystallization of a spherical domain. Fig. 13 shows the dependence of Δf on the parameter $r=R_1/R_3$ where R_3 is the radius of the spherical sample and R_1 is the radius of its internal amorphous core. The parameter r is similar to the parameter X for a cubic shape given by Eq. (3). At $r>X_{d/w}$ and at $r<X_{d/w}$ the curve $\Delta f(r)$ refers to diopside and wollastonite-like phases, respectively. According to the argumentation given above, we can suppose that at $r=X_{d/w}$ the effective thermodynamic driving force for crystallization of both phases is the same, i.e., $\Delta G_d^{eff}=\Delta G_w^{eff}$. Since $|d\Delta f_w/dr|<|d\Delta f_d/dr|$, at $r<X_{d/w}$ the effective thermodynamic driving force for growth of the wollastonite-like phase becomes higher than that for diopside and crystallization will continue via crystallization of the wollastonite-like phase. Here it should be noted that the difference between the values of Δf and hence of ΔG^{eff} for above phases is not high as compared with the thermodynamic driving force for diopside crystallization at the respective temperature (870 °C) equal to $\Delta G_d \cong 5\cdot 10^8$ J/m^3 [21].

The model employed in refs. [15,16] treats the layer of diopside crystals as a smooth one. This approach is reasonable for the second layer consisting of the wollastonite-like phase or more exactly for its internal surface. But the interface between the diopside crystal and the melt or the wollastonite-like phase is rough (see e.g. Fig. 2a). Such property of the interface is caused by the relatively large distance between crystals nucleated on surface defects. At a time corresponding to the coalescence of diopside crystals (formation of the crystalline layer) a fast increase of the density f_{cr} of elastic deformation energy can be expected to occur due to restrictions on

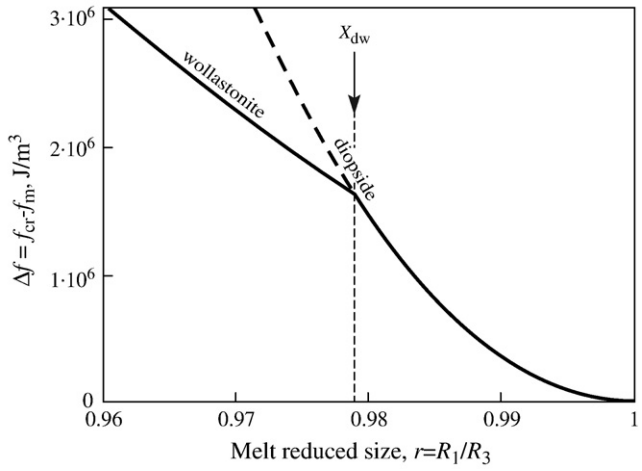

Fig. 13. Difference between densities of elastic deformation energy of crystalline and amorphous phases as a function of the parameter r calculated for the case of a sample of spherical shape. R_1 is the radius of the sphere enclosing the melt and $R_3=1$ mm is the external radius of the sample. $X_{d/w}$ corresponds to switching of phases.

elastic stress relaxation. The change of f_{cr} can be sufficiently large to trigger the growth of the wollastonite-like phase producing smaller values of f_{cr}. Thus we can suppose that the moment of coalescence corresponds to $X \cong X_{d/w}$. It could also be expected that since the growth of single crystals nucleated on glass surface is three-dimensional the average thickness of the diopside layer at the moment of its formation depends mainly on the average crystal size determined by the typical distance between the diopside crystals. Thus, by varying the size of the glass sample (from a fine powder to monolithic pieces) one can change the ratio between the amount of diopside crystals and the wollastonite-like phase in the crystallized sample, as we showed in Section 2.

The growth of the wollastonite-like phase also results in melt stretching, but to a lesser extent than for diopside. Nevertheless, such combined crystal growth finally triggers the formation of a pore, which is followed by fast growth up to a volume that, at each given moment of time, compensates in part the elastic stresses induced by the density misfit between the crystalline and glassy phases.

It should be emphasized that sometimes new crystals (hypothetically diopside) form on pore surfaces (see the crystals located around pore (3) in Figs. 2b and 12). Since the formation of a pore eliminates elastic stresses in the melt we can suppose that these crystals represent diopside. Moreover their shape is similar to that of diopside crystals on the polished surface of diopside glass giving additional support to this suggestion.

3.2. Nucleation of pores

To theoretically treat the results presented in Fig. 9, we employ classical nucleation theory (CNT). The following equation can be used for the determination of the nucleation rate, I, of pores:

$$I = I_o \exp\left(-\frac{W_* + \Delta G_D}{kT}\right), \tag{7}$$

$$I_o \approx N_1 \frac{kT}{h}. \tag{8}$$

Here N_1 is the number density of "structural units" in the ambient phase, h is Planck's constant, and T is the absolute temperature. ΔG_D is the free activation energy of attachment of "structural units" to the new phase, and W_* is the thermodynamic barrier for nucleation or the work of critical cluster formation.

Employing CNT, the work of critical cluster formation can be written in the case of pore nucleation as [9–11]

$$W_* = \frac{16\pi}{3}\frac{\sigma^3}{p^2}, \tag{9}$$

where p is the negative pressure in the stretched melt, and σ is the specific free energy of pore surface, i.e. of the melt/vacuum interface. Here it is assumed in addition that the vapor pressure in the cavitation bubble p' is small as compared to the negative external pressure p in the liquid ($|p'| << |p|$), and we thus neglect it. If one replaces, as usually done, ΔG_D by the activation energy of viscous flow, Eq. (7) can be rewritten as [22]

$$I = I_o \frac{h}{4l^3}\frac{1}{\eta}\exp\left(-\frac{W_*}{kT}\right), \tag{10}$$

where η is the viscosity of the melt and l is size parameter of order about $2 \cdot 10^{-10}$ m.

To apply the above equations to nucleation of pores one must specify the structural units, i.e. at the expense of what units in the ambient liquid phase, pore formation and growth occurs? In the case of crystalline materials, pores are considered as "negative" crystals that grow due to the attachment of vacancies [23]. These vacancies serve as "void atoms" and their number density increases under load. As opposite to a crystalline phase, the definition of vacancies in glasses, which have a structure similar to that of the liquid, is different. In this case, the holes in lattice-hole models of simple liquids could be considered as vacancies. Hereby the molar fraction of holes is taken to be equal to the relative free volume of the liquid [24]. We will use Eq. (10) assuming, to a first approximation, that the number of holes does not strongly differ from that of the structural units in the liquid, and its diffusivity can be estimated via viscosity. Some arbitrariness in the definition of the pre-exponential term, I_o, connected with these assumptions, will not strongly affect the nucleation rate.

The following equation can be written then for the number of pores nucleated in the stretched melt in a period of time t

$$N(t) = \int_0^t I(t')V(t')dt', \tag{11}$$

where I and V are the pore nucleation rate and the volume of the stretched melt, respectively. Since the negative pressure p determines, to a large extent, the thermodynamic barrier for nucleation (see Eq. (9)), its increase with increasing thickness h of the crystalline layer leads to a strong increase of the nucleation rate with heat-treatment time, t, while V weakly decreases.

Generally only *one* pore appears in a stretched melt since its fast growth eliminates the negative pressure and terminates further nucleation. That event occurs at some moment of time t_1 determined via

$$N(t_1) = 1. \tag{12}$$

Here t_1 corresponds to the critical value of X detected in experiment

$$X_* = \frac{a - 2Ut_1}{a}, \tag{13}$$

where U is growth rate of the crystalline layer.

To estimate I and then perform calculations by Eqs. (11)–(12) one needs to know the value of the negative pressure, p. In [15,16] this problem was solved for a model that treats a spherical layer of diopside as a smooth one that forms early in the crystallization process. However, as was noted in Section 3.1, in fact, the diopside crystals practically do not participate in the melt stretching. At the moment of formation of the diopside layer, when it could stretch the melt, a switch to the wollastonite-like phase occurs. Therefore, here we present results of slightly modified calculations of negative pressure for the case that the melt is stretched only by the layer of wollastonite-like phase. Hereby the thickness of the diopside crystal layer was considered as independent of the size of sample. Fig. 14 shows the results of these calculations for different radii of the sphere estimated as $R_3 = a/2$ *versus* $r = R_1/R_3$. After approaching some critical value of pressure, p_*, that corresponds to X_* i.e. formation of the pore, negative pressure drops rapidly.

In addition to the computed values of $p(r)$, experimental data on the specific surface energy, σ, and viscosity, η, were taken from refs. [25] and [21], respectively. These data allowed us to estimate the thermodynamic barrier for pore nucleation, W_*, the nucleation rate I and then the function $N(r)$ by employing CNT in the described way. The condition of pore formation is given then by the relation $N(X_*) = 1$. The comparison between theory and experiment shows that pore nucleation experimentally occurs at lower values of pressure or a smaller width of the crystalline layer than estimated theoretically. Consequently, CNT overestimates the work of critical bubble formation.

In order to arrive at a satisfactory agreement of experimental values of X_* with theoretical predictions, we have to reduce the work of critical bubble formation W_* by a factor 0.544. The results obtained

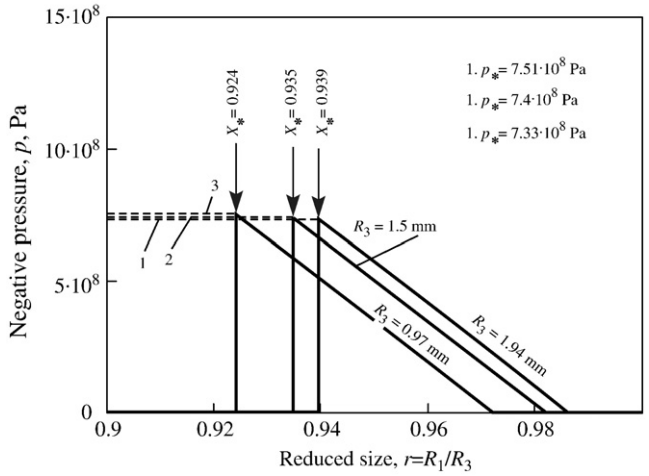

Fig. 14. Negative pressure *versus* reduced size for different sizes of spherical samples, R_3.

in such a way are shown in Fig. 11 and 15. So, the remaining question is how such reduction of the theoretically estimated thermodynamic barrier for nucleation of the pore can be explained.

3.3. Discussion

In order to give a foundation of the necessity of reduction of the work of critical bubble formation, two possibilities exist. First, employing classical nucleation theory, such deviations may be explained assuming that the specific surface energy is size-dependent, i.e., a dependence $\sigma = \sigma(R)$ is assumed. Recall that we employed in the computations the value of σ measured for a planar interface, i.e., $\sigma = \sigma_\infty$ was utilized. Since the specific surface energy in Eq. (9) refers to pores of critical radius

$$R_* = \frac{2\sigma}{p}, \tag{14}$$

the size dependence of surface energy must be taken into account. Proceeding in such a way, the work of critical cluster formation is changed according to

$$W_*(\sigma(R)) = W_*(\sigma_\infty)\left[\frac{\sigma(R)}{\sigma_\infty}\right]^3. \tag{15}$$

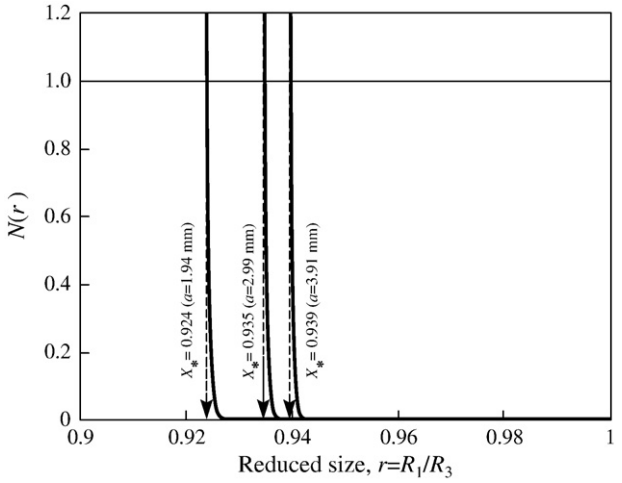

Fig. 15. Number of pores calculated by Eq. (11) for spherical sampler with size $R_3 = a/2$ heat-treated at $T = 870$ °C *versus* parameter r.

It follows that in order to reconcile theory and experiment

$$\sigma(R) = \sigma_\infty(0.544)^{1/3} = 0.816\sigma_\infty \tag{16}$$

must be assumed. The reduction of the thermodynamic barrier by a factor 0.544 can be realized via the reduction of the specific surface energy from $\sigma_\infty = 0.377$ J/m^2 [25] to $\sigma(R_*) = 0.308$ J/m^2.

To a first approximation, let us employ – with the necessary precaution (cf. e.g. [26] and the discussion below) – Tolman's equation

$$\sigma(R) = \sigma_\infty\left(1 + \frac{2\delta}{R}\right)^{-1} \tag{17}$$

for the description of the size dependence of the surface tension. Here Tolman's parameter, δ, characterizes the width of the interfacial region between the coexisting phases (it has to have the order of atomic dimensions). The required reduction of the thermodynamic barrier corresponds at a critical radius $R_* \approx 10^{-9}$ m to the reasonable value of Tolman's parameter equal to $\delta = 0.112R_* \approx 10^{-10}$ m.

However, as was shown in refs. [27–30], opposite to Tolman's equation the curvature dependence of surface tension in processes of condensation and boiling or segregation in solutions is determined by term of the order $(1/R)^2$in the expansion of σ with respect to cluster size, i.e.

$$\sigma(R) = \sigma_\infty\left(1 + \frac{B}{R^2}\right). \tag{18}$$

Assuming $B<0$ leads to a decrease of the work of critical cluster formation by a constant value as compared with the results obtained via CNT and assuming the capillarity approximation, i.e., a size-independence of the surface tension. A widely similar result was recently obtained in the analysis of crystal nucleation of certain classes of glass-forming melts [31]. Thus, in the framework of CNT, we can connect the reduction of the thermodynamic barrier for pore nucleation with the reduction of the specific surface energy due to its size dependence.

However, the question remains about the foundation of the underlying assumptions like $\delta>0$ or $B<0$. A general answer can be given by employing the generalized Gibbs approach for the determination of the work of critical cluster formation [7]. In this approach it is shown that the bulk properties of the critical clusters considerably deviate from the properties of the newly evolving macroscopic phases. As a consequence, also the specific surface energy is necessarily size-dependent. Within this approach it can be shown moreover that – under very weak assumptions concerning the systems under consideration – CNT (employing the capillarity approximation) overestimates the work of critical cluster formation. Consequently, since we employed CNT here, the theoretical values of the work of critical cluster formation are (by necessity) too high. A detailed analysis of the interpretation of pore formation in terms of the generalized Gibbs approach is in preparation.

Finally, our experiments were performed on cubes and the theoretical analysis was performed for spheres. The difference in the shapes of the samples studied theoretically and experimentally may be another origin for the quantitative deviation of theoretical and experimental results. Therefore, it would be advantageous to perform similar experiments with spherical samples or extend the theoretical computations to cubic shapes for a direct quantitative comparison with theory.

4. Conclusions

Elastic stresses, which appear due to the density misfit between the parent glass and developing crystals, strongly affect the sequence

of occurrence of crystalline phases in diopside glass. In the particular case studied here, in small cubic samples of diopside glass, diopside crystals (which are stable in non-stretched melts) form first, but their growth stops at an early stage of the phase transformation. Then nucleation and growth of a wollastonite-like crystal phase occurs. The wollastonite-like phase stretches the confined liquid to a smaller degree, than diopside crystals, due to its lower density, which is closer to the glass density.

Nevertheless, further growth of the wollastonite-like crystalline layer triggers formation of one pore, which grows fast up to a certain volume that, at a given moment of time, compensates most of the elastic stresses and eliminates the driving force for further pore nucleation. In this case, pore birth occurs in a very narrow range of negative pressures indicating that it proceeds via homogeneous nucleation. This result is corroborated by theoretical calculations of elastic stress fields. Good qualitative agreement between theory and experiment is found. However, the work of critical pore formation must be reduced to arrive at a perfect quantitative agreement with the experimental results.

The overall findings of this paper are quite general because the densities of most glasses significantly differ from those of their isochemical crystals, and are thus of great technological significance for glass–ceramic development and sinter-crystallization processes.

Acknowledgements

The authors wish to acknowledge the valuable help in the identification of the crystalline phases by the late Prof. J. F. Schepelev. We also acknowledge the financial support of the Deutsche Forschungsgemeinschaft (DFG), Germany, and Brazilian funding agencies CNPq and FAPESP — contracts 2008/00475-0 and 2007/08179-9.

References

[1] J. Möller, J. Schmelzer, I. Gutzow, Z. Phys. Chemie 204 (1998) 171.
[2] J.W. Christian, The Theory of Transformations in Metals and Alloys, Part I, Pergamon, Oxford, 1981.
[3] J.W.P. Schmelzer, R. Pacova, J. Möller, I. Gutzow, J. Non-Cystalline Solids 162 (1993) 26.
[4] J.W.P. Schmelzer, J. Möller, I. Gutzow, R. Pascova, R. Müller, W. Pannhorst, J. Non-Cryst. Solids 183 (1995) 215.
[5] J.W.P. Schmelzer, O.V. Potapov, V.M. Fokin, R. Müller, S. Reinsch, J. Non-Cryst. Solids 333 (2004) 150.
[6] J.W.P. Schmelzer, E.D. Zanotto, I. Avramov, V.M. Fokin, J. Non-Cryst. Solids 352 (2006) 434.
[7] V.M. Fokin, E.D. Zanotto, J.W.P. Schmelzer, O.V. Potapov, J. Non-Cryst. Solids 351 (2005) 1491.
[8] V.P. Skripov, V.P. Koverda, Spontaneous Crystallization of Super-cooled Liquids, Nauka, Moscow, 1984 (in Russian).
[9] V.P. Skripov, Metastable liquids, Wiley, 1974.
[10] J.W.P. Schmelzer, J. Schmelzer Jr., Kinetics of bubble formation and the tensile strength of liquids, in: J.W.P. Schmelzer, G. Röpke, V.B. Priezzhev (Eds.), Nucleation Theory and Applications, Dubna JINR, 2002, pp. 88–119.
[11] J.W.P. Schmelzer, J. Schmelzer Jr., Atmospheric Research 65 (2003) 303.
[12] S.A. Kukushkin, J. Applied Physics 98 (2005) 033503.
[13] T. Yokobori, J. Chem. Phys. 22 (1954) 951.
[14] I. Gutzow, R. Pascova, A. Karamanov, J. Schmelzer, J. Materials Science 33 (1998) 5265.
[15] A.S. Abyzov, J.W.P. Schmelzer, V.M. Fokin, On the effect of elastic stresses on crystallization processes in finite domains, in: J.W.P. Schmelzer, G. Röpke, V.B. Priezzhev (Eds.), Nucleation Theory and Applications, Dubna JINR, 2009, pp. 379–398.
[16] A.S. Abyzov, et al., Elastic stresses in crystallization processes in finite domains, J. Non-Cryst. Solids (in press), doi:10.1016/j.jnoncrysol.2010.06.014.
[17] Phase diagrams for ceramists. USA, Columbus, 1964.
[18] V.G. Baidakov, Explosive Boiling of Superheated Cryogenic Liquids, WILEY-VCH, Berlin-Weinheim, 2007.
[19] W. Hinz, Silikate, Band 1 and 2, VEB Verlag fur Bauwesen, Berlin, 1970.
[20] S. Reinsch, PhD thesis, Technische Universität Berlin, 2001.
[21] M.L.F. Nascimento, E.B. Ferreira, E.D. Zanotto, J. Chem. Phys. 121 (2004) 8924.
[22] E.D. Zanotto, V.M. Fokin, Phil. Trans. R. Soc. Lond. A (2003) 591.
[23] P.G. Cheremskoi, V.V. Slyozov, V.I. Betekhtin, Pores in the Solid State, M, Energoatomizdat, Moscow, 1990 (in Russian).
[24] I. Gutzow, J. Schmelzer, The Vitreous State: Thermodynamics, Structure, Rheology and Crystallization, Springer, Berlin, 1995.
[25] Sciglass database. http://www.esm-software.com/sciglass.
[26] A.I. Rusanov, Thermodynamic Foundation of Mechano-chemistry, Nauka, St. Petersburg, 2006 (in Russian).
[27] V.G. Baidakov, G.Sh. Boltachev, Phys. Rev. E 59 (1999) 469.
[28] V.G. Baidakov, G.Sh. Boltachev, J.W.P. Schmelzer, J. Colloid Interface Science 231 (2000) 312.
[29] M.P.A. Fisher, M. Wortis, Phys. Rev. 29 (1984) 6252.
[30] R. McGraw, A. Laaksonen, Phys. Rev. Lett. 76 (1996) 2754.
[31] V.M. Fokin, E.D. Zanotto, J.W.P. Schmelzer, Submitted for publication in J. Non-Cryst. Solids (2010).